Hindawi
International Transactions on Electrical Energy Systems
Volume 2022, Article ID 4264649, 20 pages
https://doi.org/10.1155/2022/4264649

Research Article

Control of a Three-Input DC-DC Converter Suitable for DC Motors

Amin Alizadeh Asl,[1] **Seyed Hossein Hosseini**,[1,2] **Naser Vosoughi Kurdkandi**,[3] **and Ramin Alizadeh Asl**[4]

[1]*Department of Computer and Electrical Engineering, Tabriz University, Tabriz, Iran*
[2]*Engineering Faculty, Near East University, Nicosia, North Cyprus, Mersin 10, Turkey*
[3]*Department of Electrical Power Engineering and Mechatronics, Tallinn University of Technology, Tallinn, Estonia*
[4]*Department of Electrical Engineering, Urmia University, Urmia, Iran*

Correspondence should be addressed to Amin Alizadeh Asl; aminalizadeh594@gmail.com

Received 24 November 2021; Revised 5 October 2022; Accepted 21 October 2022; Published 15 November 2022

Academic Editor: Ibrahim Mahariq

A new multivariable control technique is introduced in this paper. This method is applied to a three-input DC-DC converter. First, the dynamic model of the converter is obtained in the state space, and then, the transfer function is achieved from the state space model to design a controller. In the second step, the input-output sets must be paired using a relative gain array (RGA) matrix. In the third step, the system is decoupled in the steady state by a simple matrix. The PI controller tracks the reference inputs of the controller. If the designed controller has proper performance in the transfer function of the converter, it can be applied to a real system. This multivariable control method has suitable performance and simple implementation, which results in an inexpensive controller. The DC motor must work in a constant power region if the practical application is the aim. In this case, the torque can be directly controlled to regulate the speed of the DC motor without needing a gearbox, which promotes total efficiency. Real-time simulation and experimental results verify the effectiveness of the proposed system.

1. Introduction

In the near future, the use of PV and FC will be commonplace as renewable energy sources. A battery can also be included in the system to enhance system reliability. As power generation via PV strongly depends on environmental conditions such as temperature and solar radiation, it is essential to use a battery as a backup power source. In addition, when PV generates excess power, a battery is required to store the surplus PV energy. Without a battery, it is not possible to obtain maximum power from PV.

The control systems proposed in some studies have serious disadvantages and are thus impractical. In [1, 2], the authors proposed a new three-input DC-DC converter, besides a decoupling network for converter control. The decoupling network is one of the oldest multivariable control methods. In general, since a hybrid multiinput DC-DC converter has more than one switch, the number of inputs is more than one. Thus, based on the control theory, such power converters are multivariable systems. As a result, to control these types of power converters, a multivariable control method must be used. The most important part of a multivariable control system is coupling. In [1], in the first step, the small-signal dynamic model of the proposed hybrid multiinput DC-DC converter is achieved. In the second step, the decoupling network is obtained from the state space model. After calculating the decoupling network, an appropriate compensator is designed. Using a decoupling network creates numerous problems for the system. First, the system needs a complicated compensator. Second, the coupling loop in the decoupling network keeps the system stable within a small range of variations. Besides their difficult implementation and preservation, such control systems are extremely expensive. Still, the most significant problem is the decoupling network being noncausal; therefore, the decoupling network cannot be implemented. In other words, based on the control theory, the power electronic converter cannot decouple with this control method. Figure 1 represents the proposed control method in [1], where $G^*_{2\times2}$ is a decoupling network that can create a

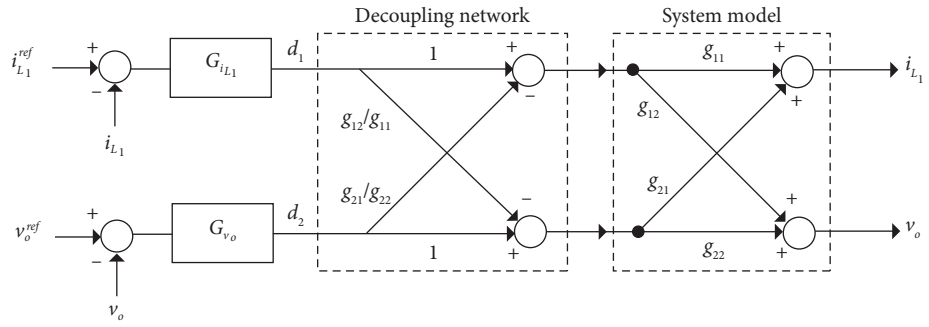

Figure 1: Decoupling control method [1].

diagonal system. Matrix (2) demonstrates the power electronic transfer function. This matrix is achieved from the state space model and shows that the decoupling network becomes noncausal in G*(2, 1). Therefore, if the Laplace inverse is applied to $G^*_{2\times2}$ to build the control system, as S (S^2) is of the second order, the system cannot be implemented in real time. Hence, this control method is inappropriate for controlling a hybrid multiinput DC-DC converter. In [3], the authors used the pole placement control method, which could be manufactured in both the inverter and the chopper mode. Their control strategy is very expensive because of the number of sensors. According to the pole placement theory, every single state variable must be fed back via a sensor, including the state variables that are not controlled. Due to measurement noise, this control method amplifies the noise. Contrary to [1, 3], in [4], the authors studied a new control method for power electronic converters. However, their solution was invalid because the small-signal dynamic model for the proposed converter was absent. To apply a control system to power electronic converters, first, a dynamic model must be obtained, and then, the performance of the controller in the dynamic model must be checked. If this performance passes verification, the control system can be applied to a power electronic converter. In [5], a novel three-input DC-DC converter was proposed, which used the structure of a conventional buck-boost at the second entrance. It increased the voltage gain of the power electronic converter, while the lack of a series inductor created a discontinuous current in the second voltage source. If the second source is a PV, it is extremely hard to perform maximum power point tracking. In [6], the main purpose was to maximize in PV and wind sources. This approach is not suitable for different applications such as a DC drive, because a DC motor is controlled by accessing the input voltage. However, their method features do not control the DC-link voltage. Similarly, in [7], besides the absence of a DC-link voltage control, there is also a time-sharing problem. As for [8], using a general control method is the advantage of the study. In contrast to [1], it uses more switches, which causes switching losses to decrease the total efficiency of the system. Similarly, in [9], there are fewer switches, but the battery is chargeable only via FC and dischargeable only via PV [1]. The first advantage of the system proposed in [10] is the sharing of switches between the half-bridge converter and boost converter, which reduces the cost. The second advantage is soft switching, which facilitates voltage gain and efficiency. Nevertheless, implementing a high frequency transformer increases the system weight. Similarly, using a high frequency transformer in [11–14] increased the system weight. In [11], the authors utilized soft-switching methods, similar to [10].

$$G^*_{2\times2} = \begin{bmatrix} 1 & -\dfrac{g_{12}}{g_{11}} \\ -\dfrac{g_{21}}{g_{22}} & 1 \end{bmatrix}, \tag{1}$$

$$G = \begin{pmatrix} \dfrac{3\times10^7 s^2 + 3\times10^{11} s + 4\times10^{13}}{s^4+112 s^3 + 5\times10^6 s^2 + 4\times10^8 s + 5\times10^{11}} & \dfrac{6\times10^4 s^3 + 3\times10^7 s^2 + 1\times10^{11} s + 1\times10^{13}}{s^4+112 s^3 + 5\times10^6 s^2 + 4\times10^8 s + 5\times10^{11}} \\ \dfrac{-8\times10^4 s^3 + 3\times10^8 s^2 - 4\times10^{11} s + 8\times10^{14}}{s^4+112 s^3 + 5\times10^6 s^2 + 4\times10^8 s + 5\times10^{11}} & \dfrac{-8\times10^{10} s + 4\times10^{14}}{s^4+112 s^3 + 5\times10^6 s^2 + 4\times10^8 s + 5\times10^{11}} \end{pmatrix}. \tag{2}$$

2. Converter Structure and State Space Average Model

Figure 2 displays the converter structure connected to the DC motor, where PV and FC are the power sources of the converter. In this structure, for the first and second sources, conventional boost and conventional buck-boost converters are, respectively, used in conjunction with a battery. The output of the converter is R-L-E, represented as an electric model of a DC motor. For proper accuracy, the mechanical part of the DC motor must be included in the model. Since PV and FC are the main power sources and only V_1 provides the DC motor current, it is necessary to select PV as V_1 or V_2. Additionally, the DC motor, as a load, needs current to provide the required torque. According to the structure, only V_1 provides the required output current ($I_o = I_{L1}(1 - d_1)$). In addition, FC has a better output current compared to PV; thus, if FC is chosen as a V_1 source, the proper performance of the converter and system will be guaranteed. Consequently, FC and PV are, respectively, designated as V_1 and V_2 sources. Nevertheless, the discontinuous current of the PV source makes maximum power point tracking a challenge in PV. To overcome this challenge, a conventional buck-boost has been allocated to the V_2 source. Therefore, I_{L2} should be controlled such that PV produces the maximum power. In this paper, the main objectives are the extraction of the maximum power from the sources and controlling the DC-link voltage in each mode. Generally, this structure has three modes. In the first mode, sources can generate the required power for the load or DC motor; therefore, the battery must be bypassed. In the second mode, the generation from sources cannot provide the load, so the control system must add battery power to the converter to supply the required power for the DC motor. In the third mode, the generation from the sources produces surplus energy that can be stored in the battery. Thus, in the third mode, the battery is charged. Each mode is divided into two operating points because the DC motor must be able to work in a constant power region without influencing the maximum tracking. In [1], the proposed converter and control system is simulated only at one operating point. However, in this study, considering the DC motor as a load, the torque must be altered to regulate the speed in each mode. Thus, each mode consists of two operating points. The second operating point is defined as torque variations to regulate the speed of the DC motor. Moreover, changing the torque should not affect the maximum.

2.1. First Operation Mode (Supplying the Load without a Battery). In the first mode, the battery must be bypassed because the generated power from the sources equates to the required power of the output stage. Since S_3, D_3, S_4, and D_4 are allocated to establish the charge and discharge paths of the battery, it can be bypassed by turning S_3 off while turning S_4 on. Based on the control theory, the duty cycle of the switches equates to control signals, i.e., adjusting the duty cycle can produce the desirable output in the converter. Due to bypassing the battery, the duty cycles of S_3 and S_4 are not considered control signals because, in this mode, $d_3 = 0$ and $d_4 = 1$. Only the duty cycles of S_1 (d_1) and S_2 (d_2) are control signals. Finally, in this mode, the main control objectives are extracting the maximum power point from the PV besides controlling the DC-link voltage. Figures 3(a)–3(c), and 4(a) demonstrate the converter operation in this mode, and (3)–(6) represent the averaged state space model of the converter in the first mode.

$$L_1\frac{di_{L1}}{dt} = -r_1 i_{L1} + (V_1 + V_C)d_1 + (V_1 - V_O)(1 - d_1), \quad (3)$$

$$L_2\frac{di_{L2}}{dt} = -r_2 i_{L2} + V_2 d_2 - V_C(1 - d_2), \quad (4)$$

$$C\frac{dV_c}{dt} = (i_{L2} - i_{L1})(d_1 - d_2) - i_{L1}d_2 + i_{L2}(1 - d_2), \quad (5)$$

$$C_o\frac{dV_o}{dt} = i_{L1}(1 - d_1) - \frac{Vo}{R_L}. \quad (6)$$

2.2. Second Operation Mode (Supplying Load by Discharging the Battery). This mode assumes that the power generated from PV and FC cannot supply the load; therefore, battery power is added to the converter. The battery discharge path can be established by turning S_4 on in this mode. By turning the S_3 on and off, the battery power can be controlled. As S_4 is kept on, the duty cycle of S_4 ($d_4 = 1$) is not a control signal, while the duty cycles of S_1, S_2, and S_3 form the control signals in this mode. Similarly, the main objectives are extracting the maximum power from the PV and FC and regulating the output voltage from the battery. Figures 3(a)–3(d), and 4(b) illustrate the converter operation in the second mode. Furthermore, (7)–(10) depict the averaged state space model of the converter in the second mode.

$$L_1\frac{di_{L1}}{dt} = -r_1 i_{L1} + V_1 + V_C d_1 + V_B d_3 - V_O(1 - d_1), \quad (7)$$

$$L_2\frac{di_{L2}}{dt} = -r_2 i_{L2} + (V_2 + V_B)d_3 + V_2(d_2 - d_3) - V_C(1 - d_2), \quad (8)$$

$$C\frac{dV}{dt} = -i_{L1}d_2 + (i_{L2} - i_{L1})(d_1 - d_2) + i_{L2}(1 - d_1), \quad (9)$$

$$C_o\frac{dV_o}{dt} = i_{L1}(1 - d_1) - \frac{V_o}{R_L}. \quad (10)$$

2.3. Third Operation Mode (Supplying Load by Charging the Battery). The generation power of PV and FC is more than the output power, so the battery must be charged in this mode. The battery can be charged by turning S_4 off in this mode. Moreover, by turning S_3 on and off, the rate of transmission power in the battery can be controlled. As a

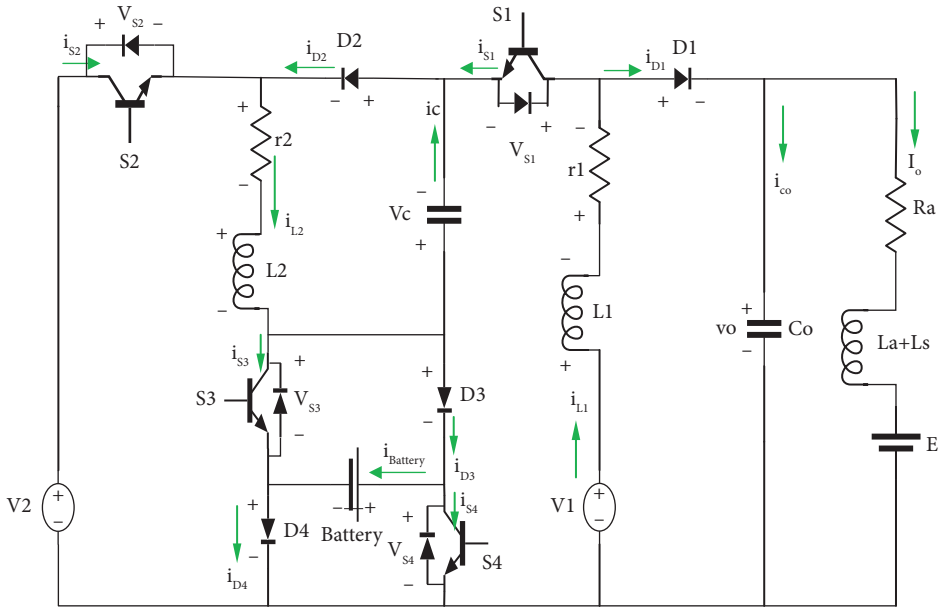

Figure 2: The suggested system for controlling the DC motor [5].

result, the duty cycle of S_4 does not act as a control signal ($d_4 = 0$). Similar to the other modes, the main control objectives are maximizing the power extracted from the PV and FC, besides regulating the output voltage. This can be achieved via control signals, the duty cycle of S_1, S_2, and S_3 (d_1, d_2, d_3). Figure 3(e)–3(g), 3(c), and 4(c) illustrate the converter operation during this mode. In addition, (11)–(14) display the averaged state space model of the converter in the third mode.

$$L_1\frac{di_{L1}}{dt} = -r_1 i_{L1} + V_1 + V_C d_1 - V_B(d_1 - d_3) - V_O(1 - d_1), \quad (11)$$

$$L_2\frac{di_{L2}}{dt} = -r_2 i_{L2} + V_2 d_3 + (V_2 - V_B)(d_2 - d_3) - V_C(1 - d_2), \quad (12)$$

$$C\frac{dV}{dt} = -i_{L1}d_2 + (i_{L2} - i_{L1})(d_1 - d_2) + i_{L2}(1 - d_1), \quad (13)$$

$$C_o\frac{dV_o}{dt} = i_{L1}(1 - d_1) - \frac{V_o}{R_L}. \quad (14)$$

3. Dynamic Modeling of the Converter in Each Mode

Equations (3)–(14) show that the power electronic converter is a nonlinear system as duty cycles are directly related to state variables, in which duty cycles control signals. In other words, by using (3)–(14), it is not possible to achieve a transfer function wherein the transfer function inputs must be control signals and the output can be state variables. By linearization at the operating point in (3)–(14), control signals and state variables can be separated, and the equations could be rewritten in a standard form. In this method, state variables, duty cycles, and inputs are divided into two components: DC values $(\overline{X}, \overline{V}, \overline{D})$ and perturbation $(\tilde{x}, \tilde{v}, \tilde{d})$:

$$x = \overline{X} + \tilde{x}\, v = \overline{V} + \tilde{v}\, d = \overline{D} + \tilde{d}. \quad (15)$$

By assuming that perturbation is small and does not significantly vary during the switching period $(\tilde{x} \ll \overline{X}, \tilde{v} \ll \overline{V}, \tilde{d} \ll \overline{D})$, by substituting (15) into (3)–(14) and excluding the second terms, small-signal models can be represented via the following matrices:

$$\dot{\tilde{x}} = A\tilde{x} + B\tilde{u}, \tag{16}$$

$$\tilde{y} = C\tilde{x} + Du, \tag{17}$$

where $\tilde{x}$, $\tilde{u}$, and $\tilde{y}$ are, respectively, the state variables vector, control variables vector, and output system. Therefore, the matrices of the small-signal models for the first, second, and third operation modes are obtained in (18)–(23).

3.1. First Operation Mode

$$\begin{bmatrix} \frac{d\tilde{i}_{L1}}{dt} \\ \frac{d\tilde{i}_{L2}}{dt} \\ \frac{d\tilde{v}_c}{dt} \\ \frac{d\tilde{v}_o}{dt} \end{bmatrix} = \begin{bmatrix} -\frac{r_1}{L_1} & 0 & \frac{\overline{D}_1}{L_1} & -\frac{1-\overline{D}_1}{L_1} \\ 0 & -\frac{r_2}{L_2} & -\frac{1-\overline{D}_2}{L_2} & 0 \\ -\frac{\overline{D}_1}{C} & \frac{1-\overline{D}_2}{C} & 0 & 0 \\ \frac{1-\overline{D}_1}{C_O} & 0 & 0 & -\frac{1}{R_L C_O} \end{bmatrix} \begin{bmatrix} \tilde{i}_{L1} \\ \tilde{i}_{L2} \\ \tilde{v}_c \\ \tilde{v}_o \end{bmatrix} + \begin{bmatrix} \frac{\overline{V}_O + \overline{V}_C}{L_1} & 0 \\ 0 & \frac{\overline{V}_2 + \overline{V}_C}{L_2} \\ -\frac{\overline{I}_{L1}}{C} & -\frac{\overline{I}_{L2}}{C} \\ -\frac{\overline{I}_{L1}}{C_O} & 0 \end{bmatrix} \begin{bmatrix} \tilde{d}_1 \\ \tilde{d}_2 \end{bmatrix}, \tag{18}$$

$$y = \begin{bmatrix} 0 & 1 & 0 & 0 \\ 0 & 0 & 0 & 1 \end{bmatrix} \begin{bmatrix} \tilde{i}_{L1} \\ \tilde{i}_{L2} \\ \tilde{v}_c \\ \tilde{v}_o \end{bmatrix}; \; D = 0. \tag{19}$$

3.2. Second Operation Mode

$$\begin{bmatrix} \frac{d\tilde{i}_{L1}}{dt} \\ \frac{d\tilde{i}_{L2}}{dt} \\ \frac{d\tilde{v}_c}{dt} \\ \frac{d\tilde{v}_o}{dt} \end{bmatrix} = \begin{bmatrix} -\frac{r_1}{L_1} & 0 & \frac{\overline{D}_1}{L_1} & -\frac{1-\overline{D}_1}{L_1} \\ 0 & -\frac{r_2}{L_2} & -\frac{1-\overline{D}_2}{L_2} & 0 \\ -\frac{\overline{D}_1}{C} & \frac{1-\overline{D}_2}{C} & 0 & 0 \\ \frac{1-\overline{D}_1}{C_O} & 0 & 0 & -\frac{1}{R_L C_O} \end{bmatrix} \begin{bmatrix} \tilde{i}_{L1} \\ \tilde{i}_{L2} \\ \tilde{v}_c \\ \tilde{v}_o \end{bmatrix} + \begin{bmatrix} \frac{\overline{V}_O + \overline{V}_C}{L_1} & 0 & \frac{\overline{V}_B}{L_1} \\ 0 & \frac{\overline{V}_2 + \overline{V}_C}{L_2} & \frac{\overline{V}_B}{L_2} \\ -\frac{\overline{I}_{L1}}{C} & -\frac{\overline{I}_{L2}}{C} & 0 \\ -\frac{\overline{I}_{L1}}{C_O} & 0 & 0 \end{bmatrix} \begin{bmatrix} \tilde{d}_1 \\ \tilde{d}_2 \\ \tilde{d}_3 \end{bmatrix}, \tag{20}$$

$$y = \begin{bmatrix} 1 & 0 & 0 & 0 \\ 0 & 1 & 0 & 0 \\ 0 & 0 & 0 & 1 \end{bmatrix} \begin{bmatrix} \tilde{i}_{L1} \\ \tilde{i}_{L2} \\ \tilde{v}_c \\ \tilde{v}_o \end{bmatrix}; D = 0. \tag{21}$$

3.3. Third Operation Mode

$$\begin{bmatrix} \frac{d\tilde{i}_{L1}}{dt} \\ \frac{d\tilde{i}_{L2}}{dt} \\ \frac{d\tilde{v}_c}{dt} \\ \frac{d\tilde{v}_o}{dt} \end{bmatrix} = \begin{bmatrix} -\frac{r_1}{L_1} & 0 & \frac{\overline{D}_1}{L_1} & -\frac{1-\overline{D}_1}{L_1} \\ 0 & -\frac{r_2}{L_2} & -\frac{1-\overline{D}_2}{L_2} & 0 \\ -\frac{\overline{D}_1}{C} & \frac{1-\overline{D}_2}{C} & 0 & 0 \\ \frac{1-\overline{D}_1}{C_O} & 0 & 0 & -\frac{1}{R_L C_O} \end{bmatrix} \begin{bmatrix} \tilde{i}_{L1} \\ \tilde{i}_{L2} \\ \tilde{v}_c \\ \tilde{v}_o \end{bmatrix} + \begin{bmatrix} \frac{\overline{V}_O + \overline{V}_C - \overline{V}_B}{L_1} & 0 & \frac{\overline{V}_B}{L_1} \\ 0 & \frac{\overline{V}_2 + \overline{V}_C - \overline{V}_B}{L_2} & \frac{\overline{V}_B}{L_2} \\ -\frac{\overline{I}_{L1}}{C} & -\frac{\overline{I}_{L2}}{C} & 0 \\ -\frac{\overline{I}_{L1}}{C_O} & 0 & 0 \end{bmatrix} \begin{bmatrix} \tilde{d}_1 \\ \tilde{d}_2 \\ \tilde{d}_3 \end{bmatrix}, \tag{22}$$

$$y = \begin{bmatrix} 1 & 0 & 0 & 0 \\ 0 & 1 & 0 & 0 \\ 0 & 0 & 0 & 1 \end{bmatrix} \begin{bmatrix} \tilde{i}_{L1} \\ \tilde{i}_{L2} \\ \tilde{v}_c \\ \tilde{v}_o \end{bmatrix}; \; D = 0. \tag{23}$$

4. Open-Loop Analysis and Pairing the Input-Output Set

According to (24), the state space model can be turned into a transfer function. Further, (24) can determine the size of the transfer function matrix. In the first mode, we have $[A]_{2\times2}$, $[B]_{2\times2}$, $[C]_{2\times2}$; therefore, the transfer function is $[G]_{2\times2}$. Similarly, in the second and third modes, the transfer function is $[G]_{3\times3}$:

$$G = C(sI - A)^{-1}B + D. \tag{24}$$

Since the transfer function is a square matrix in each mode, the power electronic converter is a multivariable system, as expected. Due to the squareness of the matrix, the system does not have the problems of a nonsquare system. The most significant problem of the multivariable system is system coupling, i.e., the output gains a value even with zero inputs. Equation (25) describes the system in the first mode, where the system has two outputs: Y_1 and Y_2 are I_{L2} and V_O, respectively; I_{L2} must be controlled to extract the maximum power of PV, and V_O must be controlled to control the DC motor. According to (25), if u_2 becomes zero, Y_2 will not be zero and retains a significant value ($y_2 = g_{21}u_1$); this phenomenon in the second output is called coupling. In other words, coupling in the output stage does not allow the system to be controlled independently.

$$\begin{bmatrix} y_1 \\ y_2 \end{bmatrix} = \begin{bmatrix} g_{11} & g_{12} \\ g_{21} & g_{22} \end{bmatrix} \begin{bmatrix} u_1 \\ u_2 \end{bmatrix}, \tag{25}$$

$$y_1 = g_{11}u_1 + g_{12}u_2 \xrightarrow{u_2 = 0} y_1 = g_{11}u_1, y_2 = g_{21}u_1 + g_{22}u_2 \xrightarrow{u_2 = 0} y_2 = g_{21}u_1. \tag{26}$$

In the multivariable system, when the system is 2×2, the input $[u]^T = [1\ 0]$ is given to the system, and in this state, the second output value is affected by coupling. Figure 5 shows the open loop performance of the system in the first mode. When the input is $[u]^T = [1\ 0]$, the value of Y_1 is approximately 70, whereas the value of Y_2 reaches 1500 even though the second input is zero. As expected, the system has a strong coupling. Similarly, Figures 6 and 7 depict the open loop behavior of the system in the second and third modes, respectively, with strong coupling.

As the first step in a multivariable control system, we need to pair a suitable input-output set. Nowadays, in multivariable control, this is performed via a relative gain array (RGA) matrix. The RGA matrix can be achieved as follows:

$$\Lambda(G(j\omega)) = G(j\omega). * G(j\omega)^{-T}. \tag{27}$$

In the first mode, the system has two outputs and two control signals; consequently, we have two options: for controling the outputs. If pairing is carried out via the RGA matrix, control system difficulties will be improved.

The RGA matrix in the first operation mode:

$$\mathrm{RGA} = G. * G^{-T} = \begin{bmatrix} 4.04 & -3.04 \\ -3.04 & 7.04 \end{bmatrix}. \tag{28}$$

According to the RGA matrix in (28), it is clear that by closing the second loop, the gain between Y_1 and u_1 declines because RGA (1, 2) is negative. If the first loop is closed, the gain between Y_2 and u_2 declines since RGA (2, 1) is negative.

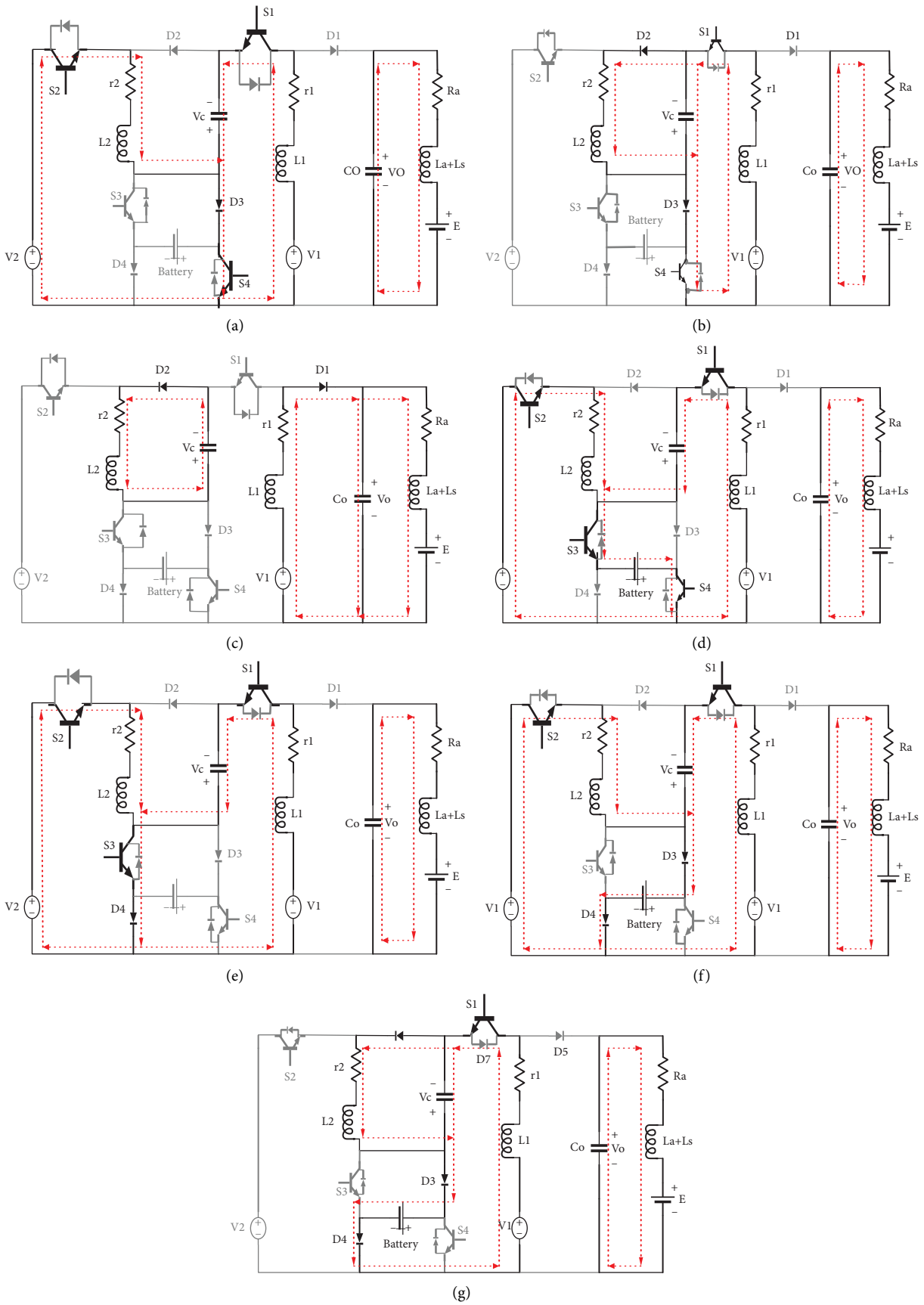

Figure 3: All operation modes of the hybrid DC-DC converter.

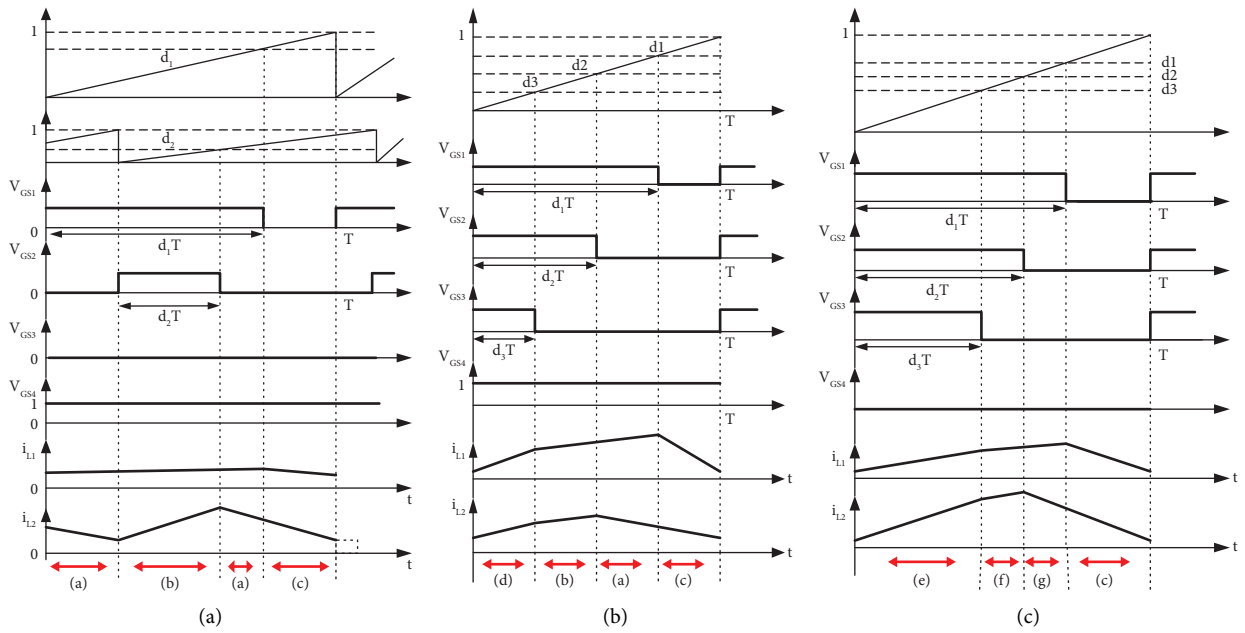

Figure 4: The order of switching in all three modes: (a) First operation mode; (b) second operation mode; (c) third operation mode.

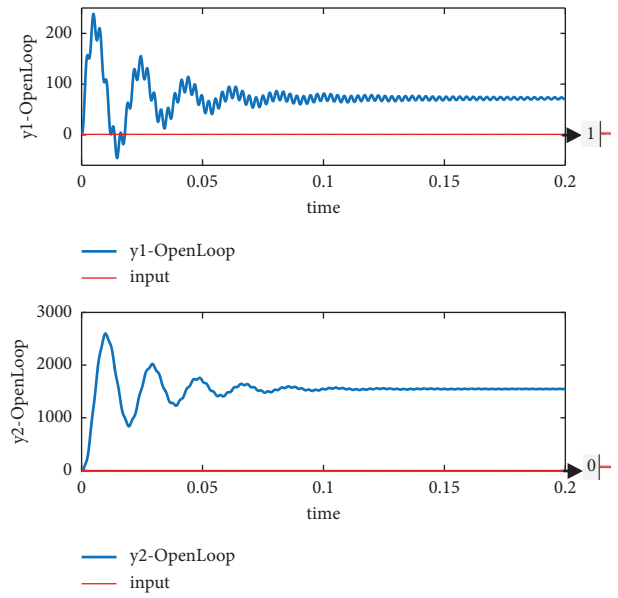

Figure 5: System response in the first mode to input $[u]^T = [1\ 0]$.

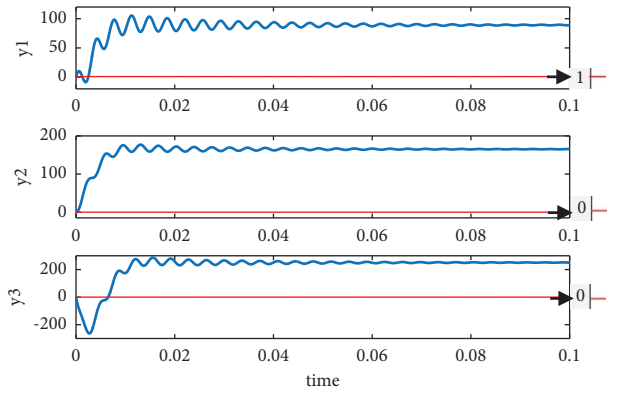

Figure 6: System response in the second mode to input $[u]^T = [1\ 0\ 0]$.

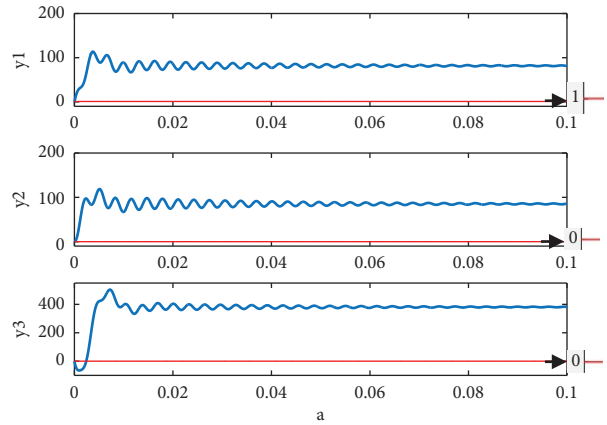

Figure 7: System response in the third mode to input $[u]^T = [1\ 0\ 0]$.

As a result, the system has strong coupling. Moreover, in the open loop analysis, the strong coupling of the system was detected. Since diagonal elements are positive and more than nondiagonal elements in the RGA matrix above, it can be concluded that the first control signal (u_1) has the greatest impact on the first output (Y_1); further, the second control signal (u_2) has the strongest effect on the second output (Y_2). As such, the best option for pairing in the first mode is $u_1 \longrightarrow y_1\, u_2 \longrightarrow y_2$.

The output must be controlled with positive elements in the RGA matrix. If nondiagonal elements are more than diagonal elements in the RGA matrix above, despite u_2 having the strongest effect on Y_1, due to being negative, Y_1 must be controlled with u_1. Because being negative causes a 180° phase difference, it increases system instability. Generally, positiveness is prioritized in the RGA matrix method.

The RGA matrices in the second and third operation modes are as follows:

$$\text{RGA} = \begin{bmatrix} 2.18 & -1.56 & 0.38 \\ -0.0008 & 1.78 & -0.78 \\ -1.18 & 0.79 & 1.49 \end{bmatrix}, \text{RGA} = \begin{bmatrix} 1.83 & -1.21 & 0.37 \\ -0.0006 & 1.72 & -0.72 \\ -0.83 & 0.48 & 1.35 \end{bmatrix}. \tag{29}$$

Similarly, the best options for pairing in the second and third modes are $u_1 \longrightarrow y_1\, u_2 \longrightarrow y_2\, u_3 \longrightarrow y_3$

5. Closed-Loop Configuration and Performance

Based on the open loop analysis section, the extreme coupling may mean that system outputs are not independently controllable. In the decentralized control method (a famous multivariable control technique), the compensator matrix must be chosen such that the system has diagonal dominance. In other words, non-diagonal elements should not affect the system. Nowadays, in multivariable control, the compensator matrix is chosen such that the system maintains diagonal dominance in the steady state. Selecting CP as a compensator matrix depends on the system and control objectives. Many compensators have been proposed for multivariable controllers in the multivariable control theory, but in this study, as the steady state of the power electronic converter is important, the compensator matrix (CP) is chosen as follows:

$$\text{CP} = [G(0)]^{-1}. \tag{30}$$

If (30) is used as a compensator matrix, the system becomes decoupled in the steady state, as CP is positioned before the system. However, if the system is to feature diagonal dominance in a varying frequency range, CP can be chosen as follows:

$$\text{CP} = j\omega_b \left[G\left(j\omega_b\right)\right]^{-1}. \tag{31}$$

Equations (30)-(31) are completely static, which reduces the cost of the control system, although the CP can be designed dynamically. Still, in this case, besides the control system cost, the control system becomes further complex. If a simple static matrix can provide suitable performance, it is not necessary to use a complex CP. Accordingly, (30) is used to create diagonal dominance in the steady state. The PI coefficients must be chosen such that the closed-loop system is stable and able to track reference inputs. Figure 8 illustrates the closed-loop configuration of the first mode, and Figure 9 depicts the closed-loop configuration in the second and third modes.

Open-loop analysis indicated that system coupling does not allow the outputs to be controlled independently. The compensator matrix (CP) is chosen from (30) to decouple the system in the steady state, and the PI controller is added to the system to track reference inputs. According to Figures 8 and 9, the chief advantage of this configuration—besides low cost—is that, with a simple static matrix and a diagonal PI controller, the control system can properly control a complex system too. Using MATLAB software, the system was simulated and the performance of the closed loop was acquired in each mode.

Figure 10 demonstrates the system step response, showing that the system is decoupled in the steady state, and the outputs are controlled independently when $[u]^T = [1\ 0]$, where y_2 remains zero. Moreover, y_1 also reaches the expected value. In the second moment, u_1 varies while u_2 remains zero, and y_1 can reach the expected value.

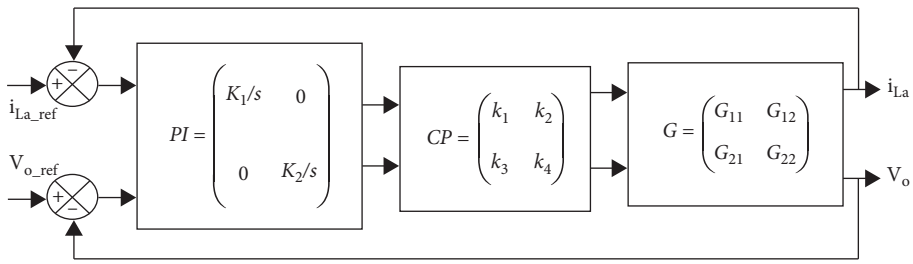

Figure 8: Scheme of the closed loop in the first mode.

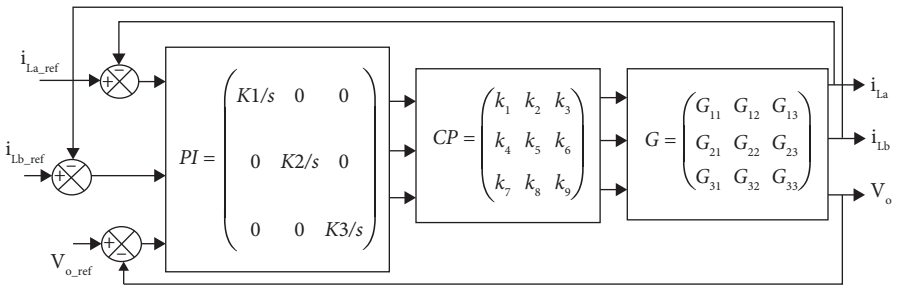

Figure 9: Scheme of the closed loop in the second and third modes.

In the open-loop analysis, although $u_2 = 0$, y_2 has a significant value. This control method solves all the problems of the multivariable control system; therefore, system coupling is properly controlled and reference inputs' tracking is performed in line with the proposed configuration. A decentralized control technique provides the desired output and performance, despite the complexity of the transfer function. Figures 11 and 12 show the closed-loop performance for the second and third modes, respectively.

6. Comparison

Numerous DC-DC converters were cited in the references. The decoupling network and pole placement control theory have been employed to control DC-DC converters. The decoupling control technique cannot be applied to all DC-DC converters because, based on (2), there is a possibility that the decoupling network becomes noncausal. According to the pole placement control theory, all state variables must be fed back via sensors. This technique implements numerous sensors, which raises the control system costs while reducing system reliability. Only these control methods have been employed to control the MIMO or MISO converters; therefore, a superior multivariable control technique needs to be proposed and utilized. Reference [15] scrutinized different multivariable control techniques. Thus, this paper employs the decentralized control technique as a well-known multivariable method [16, 17] to control the DC-DC converter, wherein the required state variables must be fed back and, thus, fewer sensors are required. Tables 1–3 compare the decentralized control method with other techniques.

7. Simulation Results

Three operation modes are simulated with MATLAB/SIMULINK. This hybrid multiinput DC/DC converter must be able to control the DC motor as a load. The key parameter of the simulation is that the DC motor must be able to operate in a constant power region in all three operation modes. If the torque changes, speed must be regulated such that the maximum power points are not affected. A series DC motor is used in three operation modes. In a series DC motor: $T_L = K.i_a^2$; therefore, it requires torque that can be provided with a lower current in comparison to the other DC motor. Moreover, this lower current reduces converter conductivity losses. For simplicity, the DC machine constant $K = 1$ is assumed in all three operation modes. Figure 13 shows the general scheme of the proposed system to drive a DC motor. Tables 4 and 5 present the simulation parameters.

7.1. First Mode. In the proposed system, the power generated by PV and FC and the required DC motor torque are system inputs. Figure 14 illustrates system inputs in the first operation mode, where the maximum powers of PV and FC are 400 W and 600 W, respectively. Figure 14(a) shows the PV characteristic and Figure 14(b) shows the FC characteristic. The required torque is 5.5 N·m as demonstrated in Figure 14(c); however, in the second moment, torque is altered to 90.5 N·m. As the power generation of PV and FC remains constant, according to $P = T.\omega$, if torque is altered, speed must be regulated. This step change in torque should not affect the maximum power point tracking. Altering the torque is required for speed control. In this operation mode, the control objectives were maximizing the power generated by PV and regulating the output voltage. Due to the conventional buck-boost converter at the inlet of the PV, direct PV control is impossible. According to $I_{PV} = d_2$. I_{L2}, the I_{L2} can be controlled such that the maximum power point tracking is achieved from PV. The RGA matrix showed that the first and the second outputs must be controlled with the first and the second control signals, respectively ($I_{L2} \longrightarrow d_1$, $V_O \longrightarrow d_2$). Figure 14 shows the maximum power point of PV is in 60 V. At close to 19 A or 31 V, the FC

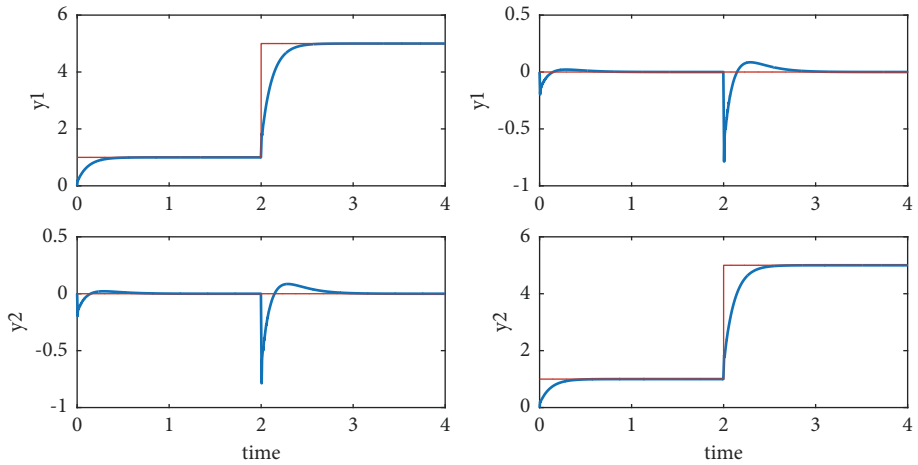

Figure 10: System step response in the first mode.

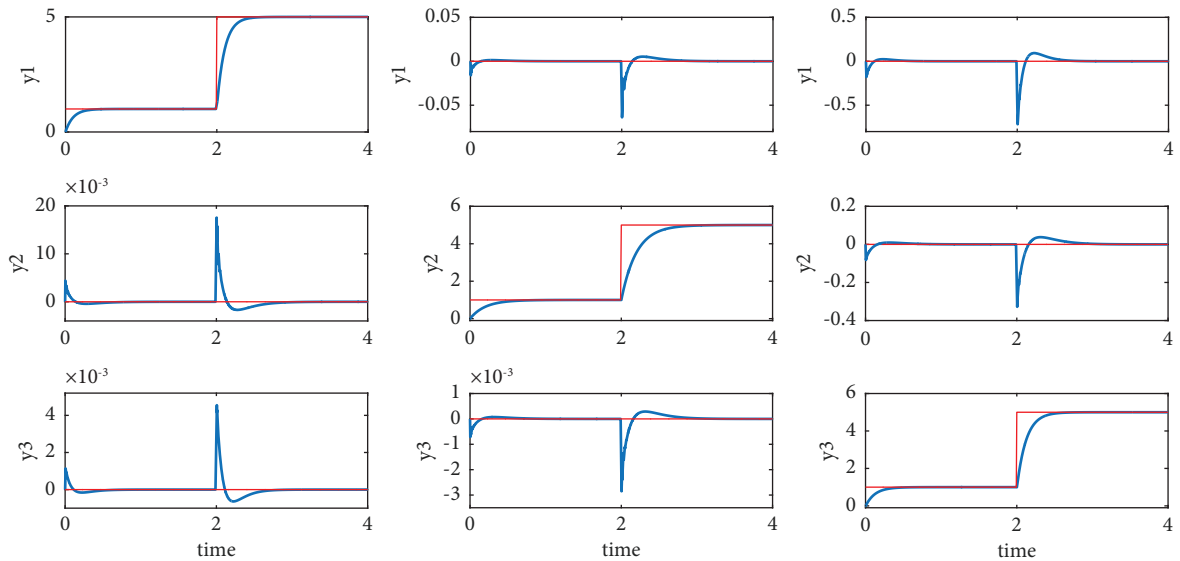

Figure 11: System step response in the second mode.

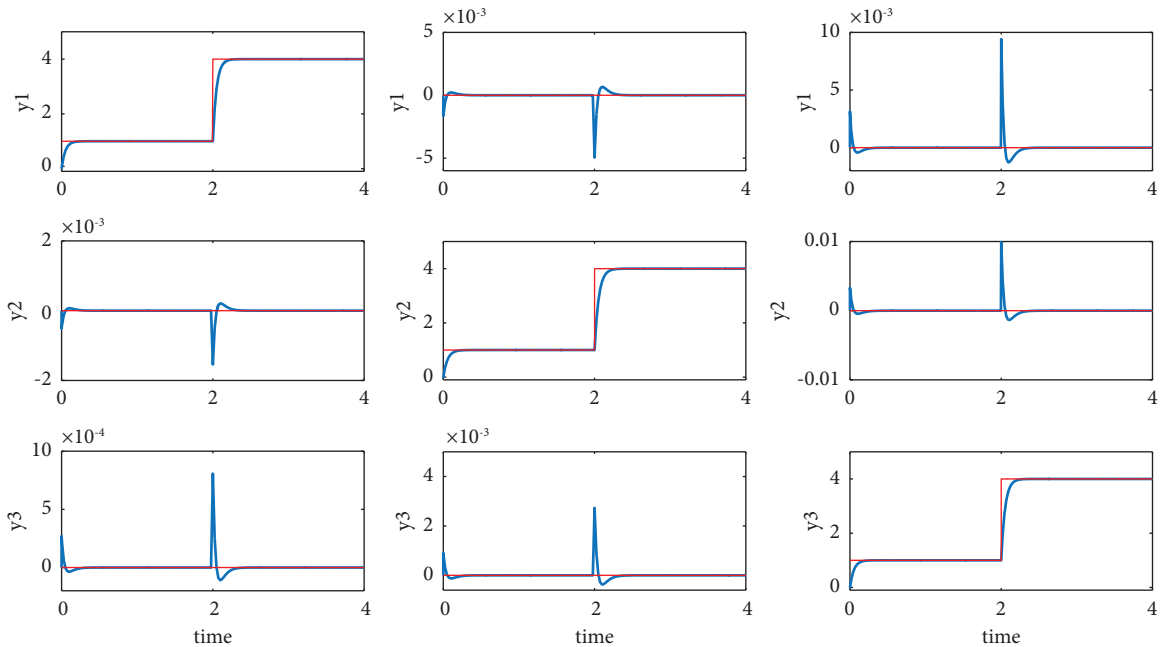

Figure 12: System step response in the third mode.

Table 1: Superiority of the proposed control method compared to the pole placement technique.

References	The used control method	The sensors needed when the pole placement method is utilized	The sensors needed if the proposed control is utilized
[18]	Pole placement	6	2
[19]	Pole placement	5	2
[2]	Pole placement	8	5
[20]	Pole placement	11	4

Table 2: Superiority of the proposed control method compared to the decoupling network technique.

References	The used control method	The requirements of the decoupling network control	The requirements of the proposed control method
[1]	Decoupling network	Needing a nondiagonal extra decoupling network, existence of an intricate controller	Needing a diagonal PI controller, existence of a simple compensator
[21]	Decoupling network		
[22]	Decoupling network		
[23]	Decoupling network		

Table 3: Advantages of the proposed control in extendable multiinput DC-DC converters.

References	The converter with extendibility features (stages)	The sensors needed if the pole placement control method is utilized	The sensors needed if the proposed control method is utilized
[19]	N	2N + 1	N + 1
[20]	N	2N + 3	N
[2]	N	N + 4	N + 1
[24]	N	N + 3	N
[25]	N	2N + 2	N

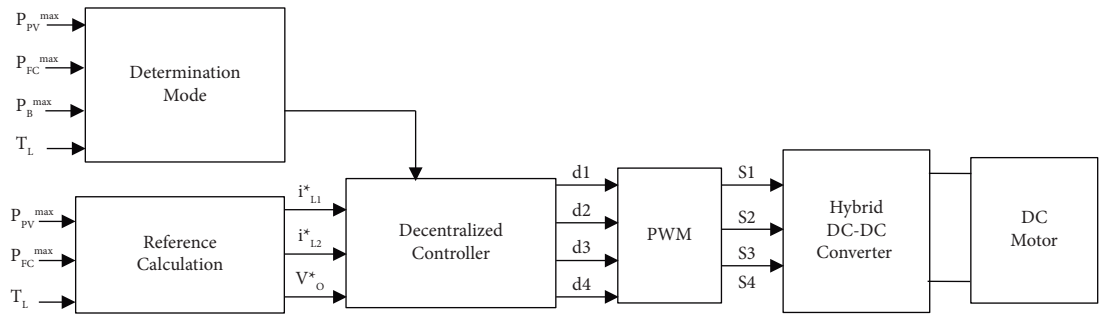

Figure 13: General scheme of the proposed system.

Table 4: Converter simulation parameter.

Symbols	Parameter
$r_1 = r_2$	0.1Ω
$L_1 = L_2$	1.5 mH
C	40 μF
C_{out}	80 μF
f_s	25 kHz

Table 5: DC motor parameter.

Symbol	Parameter
Ra	1Ω
La	0.5 mH
Ls	0.5 mH
J	0.01 kg/m^3
K	1

power is maximized. Figure 15 indicates that the control signals (duty cycles) have been altered to meet the control objectives; thus, the control system operates accurately because the maximum power of the sources is tracked while supplying the required torque. Figure 15(a) shows the duty cycle of S_1, and Figure 15(b) displays the duty cycle of S_2. According to Figure 16, despite the step change of torque in the second moment, maximum power point tracking is achieved. Figure 17(a) implies that I_{FC} (I_{L1}) remains 19 A despite the step change in torque; hence, the maximum power of FC is achieved. Moreover, due to operating in a constant power region, V_O in Figure 17(c) is reduced to

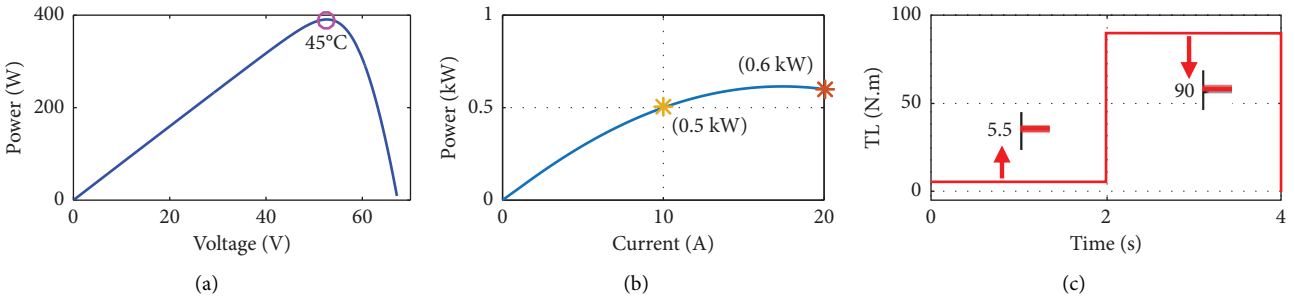

Figure 14: Systems inputs in the first operation mode. (a) PV characteristic, (b) FC characteristic, and (c) torque.

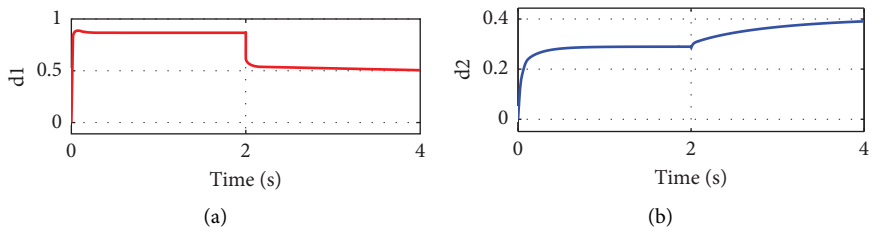

Figure 15: Duty cycles in the first operation mode. (a) Duty cycle of S1 and (b) duty cycle of S2.

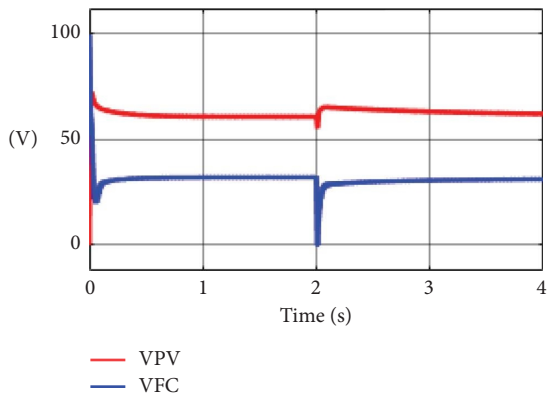

Figure 16: V_{PV} and V_{FC} in the first operation mode.

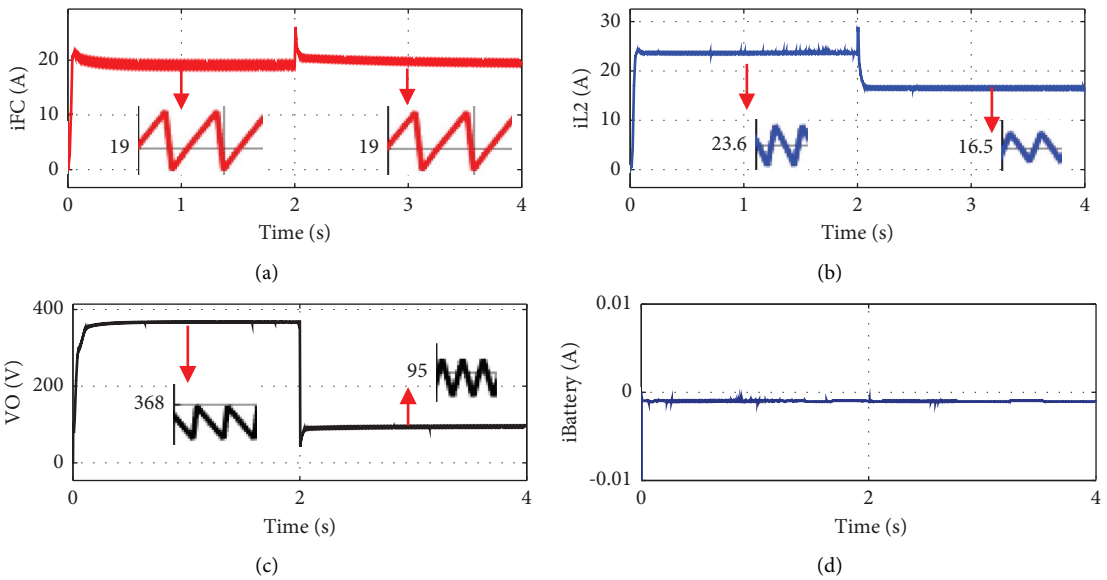

Figure 17: DC-DC converter specifications. (a) Current of FC, (b) current of iL2, (c) output voltage, and (d) current of battery.

provide the required torque. In addition, $I_{PV} = d_2.I_{L2}$ and due to the maximum power point tracking, I_{PV} must be constant during this mode. However, I_{L2} is controlled by d_1, but if d_2 increases, then I_{L2} must decrease. It can be claimed that the control system functions properly, as shown in Figure 15(b) and 17(b). Furthermore, the battery is bypassed in this mode; consequently, the current of the battery must be zero, as shown in Figure 17(d). Finally, Figure 18(b) depicts the speed of the series DC motor. In the second moment, torque is changed. As the power generated by the source remains constant, and considering the basic equation $P = T.\omega$, the speed must be altered or regulated. When $T_L = 5.5$ N·m, the required current is 2.3 A because $K = 1$. Figure 18(a) shows that the armature current has increased to around 9.5 A. Therefore, the required torque of the DC motor is supplied. As explained in Section 2, the importance of source selection is confirmed here. Figure 14(a) indicates the maximum power of 400 W occurring at a voltage of 60 V. Therefore, the maximum current is 6.6 A in PV. On the other hand, the required torque at the second moment is 90.5 N·m. In the series of DC motors: $T_L = K.i_a^2 \longrightarrow^K = 1\ T_L = i_a^2$. For a torque of 90.5 N·m, a current of 9.5 A is needed, which is impossible for PV to provide. This is why FC and PV have been chosen as V_1 and V_2 sources, respectively.

7.2. Second Mode. Figure 19(a) and 19(b) show that PV and FC have similar characteristics to the previous mode. Only a battery is added to the system to increase the output power. As such, this mode can be classified as an acceleration region in the DC motor, i.e., if the PV and FC cannot generate enough power, the battery will be added to the system. According to Figure 19(c), the power of the battery is assumed to be 500 W. Hence, the total power generated by sources is 1.5 kW, which must supply the output power and the converter losses. Further, in Figure 19(c), the torque is changed in the second moment; however, in contrast with the previous mode, here the torque is reduced in the second moment. The torque has been chosen in a completely arbitrary manner. In this mode, control objectives include extracting the maximum power from sources and adding a battery to the system to regulate the output voltage. By controlling I_{L1} and I_{L2}, it is possible to maximize the power of the FC and PV, respectively. In the same way, the output voltage can be controlled through the output capacitor. The RGA matrix showed that I_{L1}, I_{L2}, and V_O, respectively, with d_1, d_2, and d_3, must be controlled ($I_{L1} \longrightarrow d_1$, $I_{L2} \longrightarrow d_2$, $Vo \longrightarrow d_3$). Similar to the first operation mode, Figure 20 indicates that the control signal is accordingly changed to extract the maximum power from sources and provide the required torque. Figures 20(a)–20(c) show the duty cycle of S_1, S_2, and S_3, respectively. Figure 21 implies that in the second moment, maximum power point tracking from the sources is achieved despite the step-changing of the torque. Another cause of the maximized power point tracking in the FC is that I_{L1} (I_{FC}) remained close to 19 A (Figure 22(a)). Moreover, when I_{L2} increases (Figure 22(b)), d_2 decreases (Figure 20(b)), indicating that according to $I_{PV} = d_2.I_{L2}$, the I_{PV} remains constant, and the torque step-changing does not affect the maximum power point tracking in PV. Additionally, Figure 21 clearly shows that the maximum power point is tracked. Due to operating in a constant power region, V_O increases (Figure 22(c)) to provide the required current or torque. In Figure 22(d), the current of the battery is negative, meaning that the battery is discharged, and power runs from the battery to the load. The current and speed of the series DC motor is depicted in Figure 23. Figures 23(a) and 23(b) show the armature current and speed of the DC motor, respectively. In this circumstance, like the first operation mode, the positions of PV and FC are of key importance. Until the second moment, torque is 87.5 N·m and as $K = 1$, the series DC motor requires a current of 9.5 A; nevertheless, the PV cannot provide it. Therefore, the first source must be FC, while the second source must be PV. Although this positioning means that PV has a discontinuous current, using I_{L2} to control PV solves this problem.

7.3. Third Mode. In this operation mode, PV power generation rises, and the surplus energy is stored in the battery. Therefore, in this mode, the battery current is positive. Figure 24 shows the system inputs in the third mode, where the maximum powers of PV (Figure 24(a)) and FC (Figure 24(b)) are 1.2 kW and 600 W, respectively, with corresponding voltages of 90 V in PV, and 31 V or 19 A in FC. Figure 24(c) depicts the required torque and nominal power of the battery in this mode. The duty cycles are demonstrated in Figure 24. Figure 25(a), (b), (c) show the duty cycle of S_1, S_2, and S_3, in that order. Figure 26 shows that the maximum power point is tracked despite the step-changing of the torque; Figure 27 depicts that the maximum power point is tracked in the FC due to the stability of I_{L1} (Figure 27(a)); and as shown in Figure 28, the DC motor is controlled properly at variable speeds (Figure 28(b)) without affecting the maximum powers of PV and FC. Figure 27(c) confirms that the output voltage is decreased to provide the needed torque. Furthermore, the positive current of the battery in Figure 27(d) reveals that the battery is charging. Moreover, I_{L2} decreases (Figure 27(b)) when d_2 rises (Figure 25(b)), suggesting that PV reaches the maximum power and the control system performs well. Finally, Figure 28(a) shows the DC motor current. Similar to the other modes, all control objectives are achieved.

8. Experimental Results

To verify the effectiveness of the converter, a high-power laboratory prototype was built in the 800 W range, as shown in Figure 29. Two sources were used in this hardware setup. Because of the low output voltage of the FC in comparison with PV, V_1 was set to 60 V and V_2 was set to 180 V. The voltage and current of sources are depicted in Figures 30. In Figure 31, the measured output voltage and current are, respectively, 370 V and 2.16 A. In addition, the voltage of the second capacitor is displayed in Figure 31. Figure 32 shows

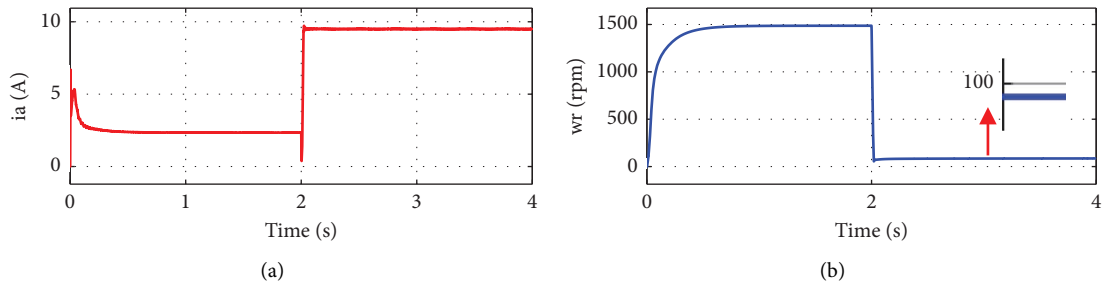

FIGURE 18: Series DC motor specifications. (a) Armature Current and (b) speed of DC motor (rpm).

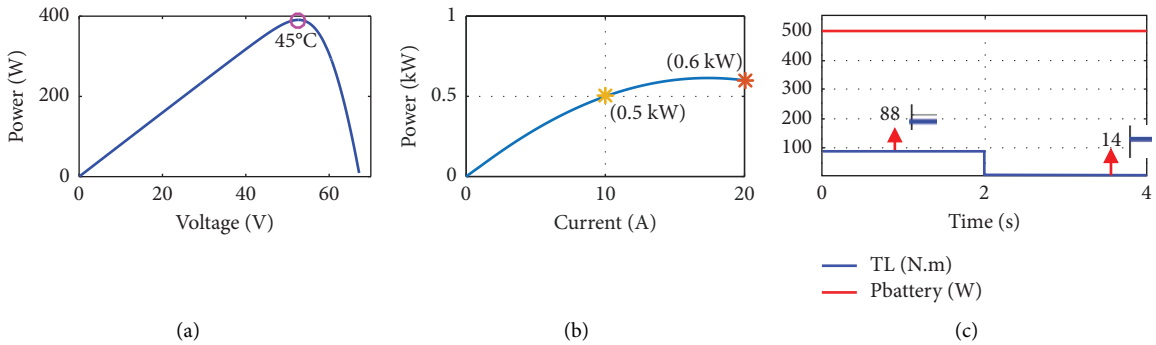

FIGURE 19: System inputs in the second operation mode. (a) PV characteristic. (b) FC characteristic. (c) Torque and nominal power of the battery.

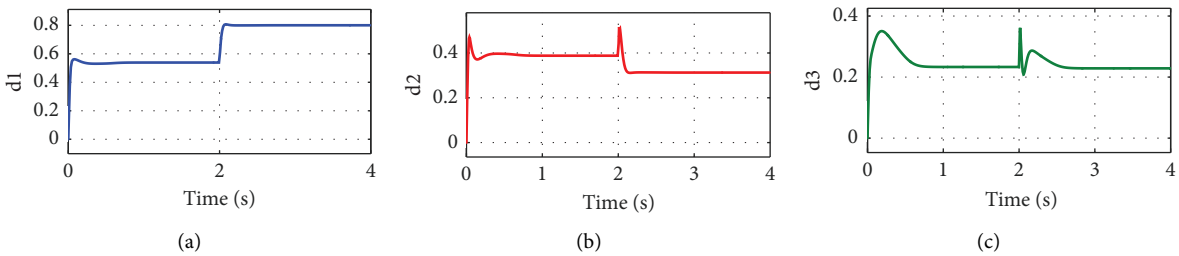

FIGURE 20: Duty cycles in the second operation mode. (a) Duty cycle of S1, (b) duty cycle of S2, and (c) duty cycle of S3.

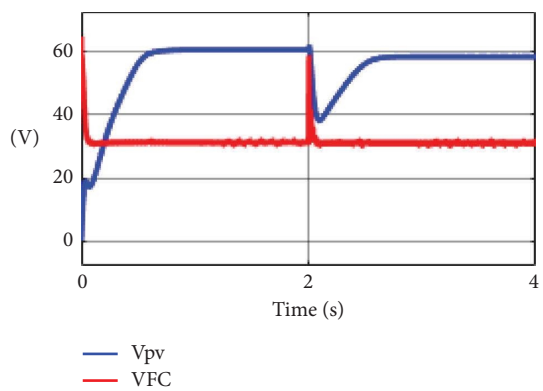

FIGURE 21: V_{PV} and V_{FC} in the second operation mode.

the voltage of switches and diodes. Figure 33 shows the dynamic response of the suggested converter. Figures 33(a) and 33(b) confirm the result of the simulation, which means that when the load varies, the output voltage is regulated to extract the maximum power from the sources. This function enables the extraction of the set power.

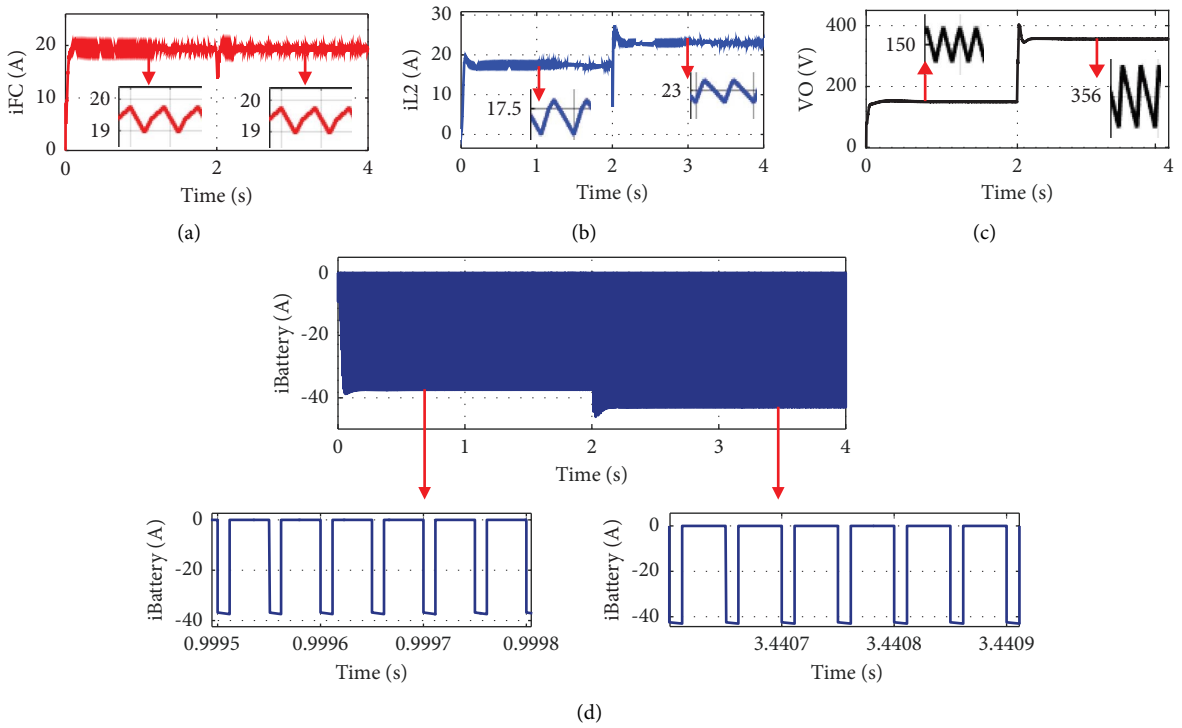

Figure 22: DC-DC converter specification in the second mode. (a) Current of FC, (b) current of iL2, (c) output voltage, and (d) current of battery.

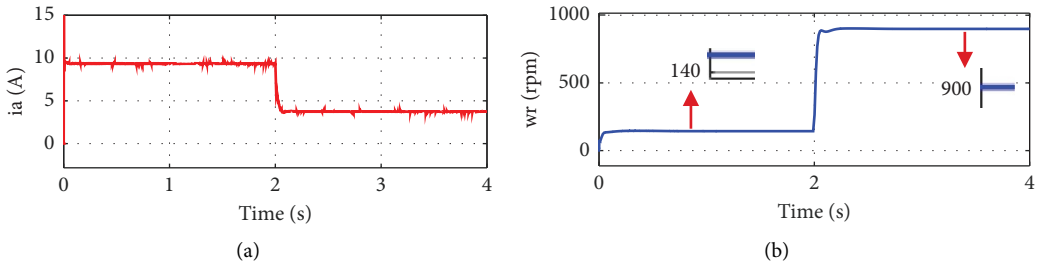

Figure 23: Series DC motor specification in the second mode. (a) Armature current and (b) speed of DC motor (rpm).

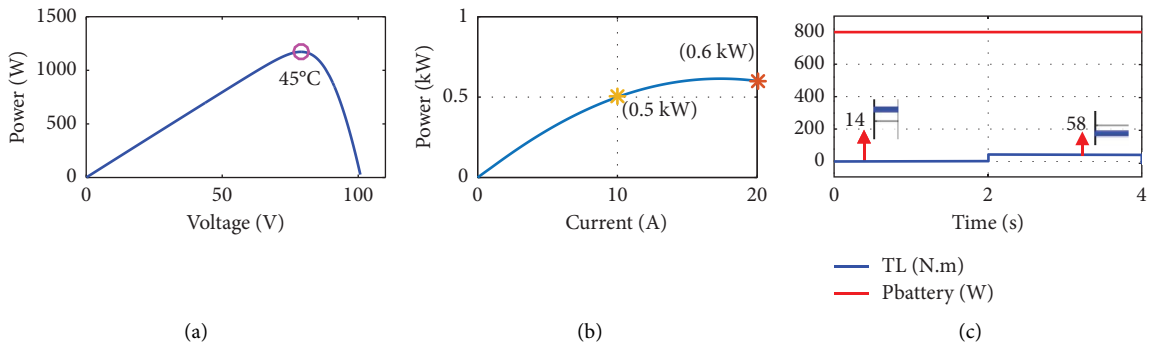

Figure 24: System inputs in the third operation mode. (a) PV characteristic. (b) FC characteristic. (c) Torque and nominal power of the battery.

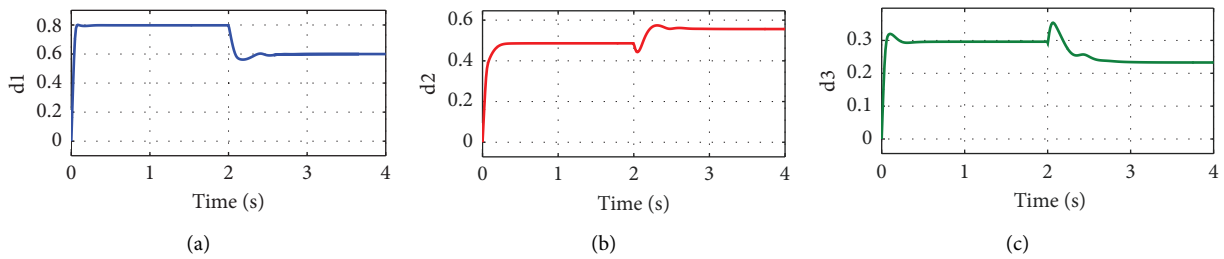

Figure 25: Duty cycles in the third operation mode. (a) Duty cycle of S1. (b) Duty cycle of S2. (c) Duty cycle of S3.

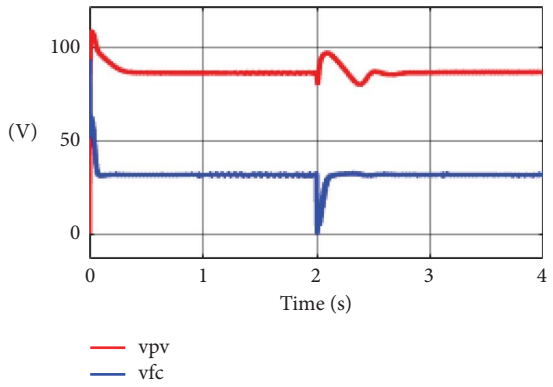

Figure 26: V_{PV} and V_{FC} in the third operation mode.

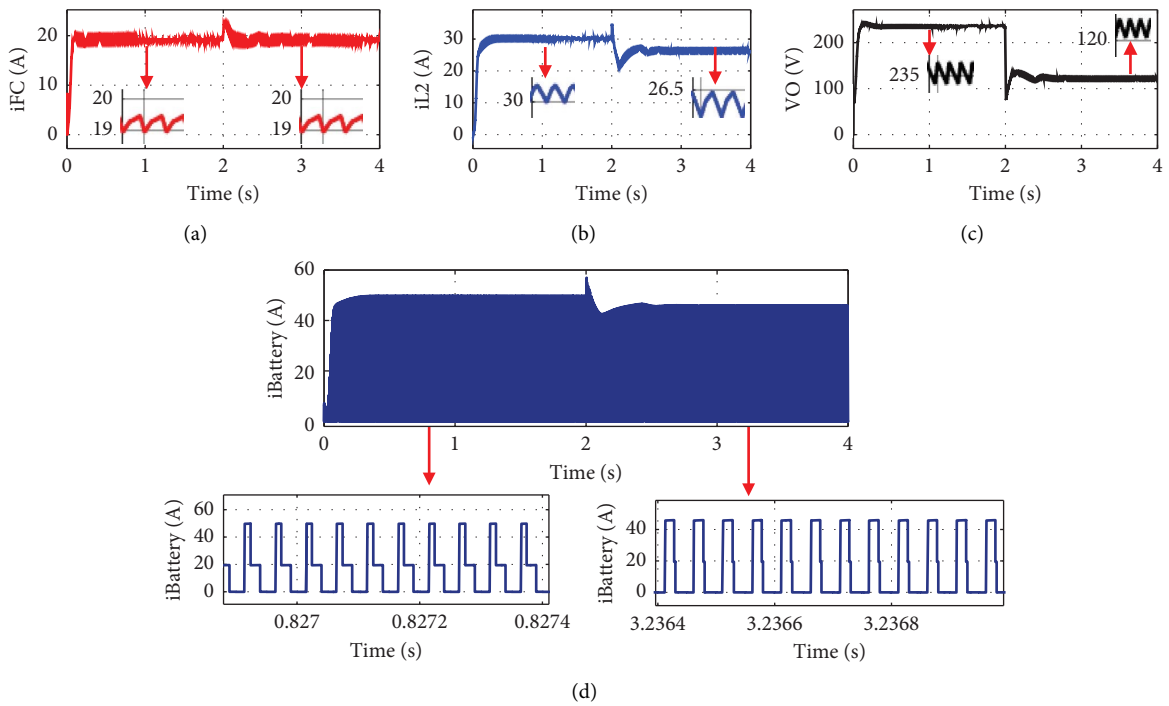

Figure 27: DC-DC converter specifications in the third mode. (a) Current of FC. (b) Current of iL2. (c) Output voltage. (d) Current of the battery.

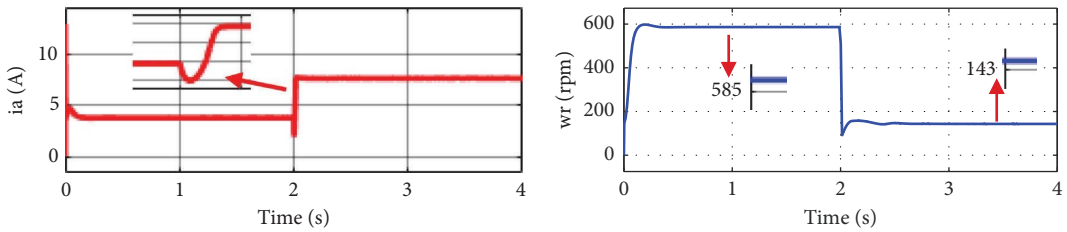

Figure 28: Series DC motor specification in the third mode. (a) Armature current. (b) Speed of DC motor (rpm).

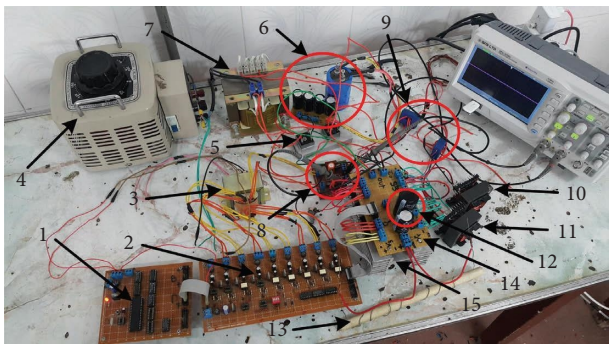

Figure 29: Experimental prototype.

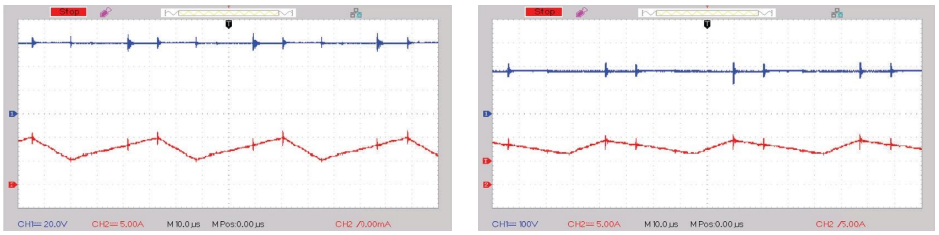

Figure 30: (a) Voltage and current of the first source. (b) Voltage of the second source and current of the second inductor.

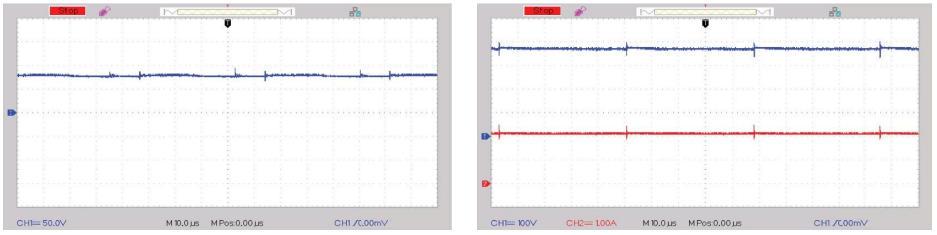

Figure 31: (a) Capacitor voltage. (b) Voltage and current of the load.

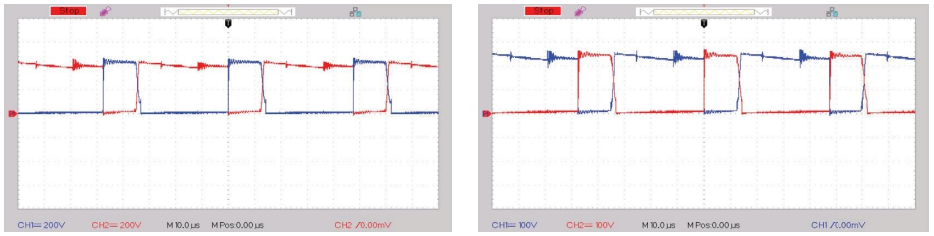

Figure 32: (a) Voltage of S_1 and D_1. (b) Voltage of S_2 and D_2.

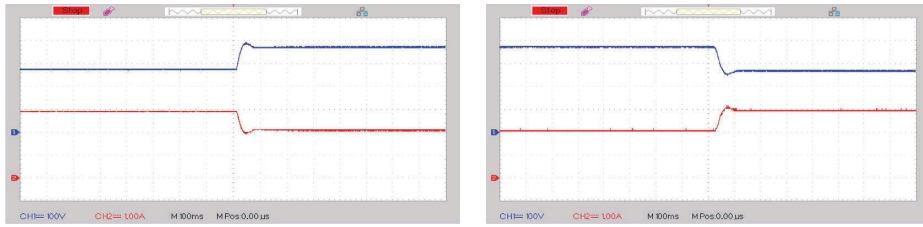

(a) (b)

Figure 33: Dynamic response of the suggested converter. (a) Increasing output voltage. (b) Decreasing output voltage.

9. Conclusion

Multiinput DC-DC converters will be more common in the future with the increasing application of renewable energies such as PV and FC. Hence, it is vital to control such converters with proper control techniques. Moreover, controlling the DC motor is essential in practical applications. In this paper, a three-input DC-DC converter with PV, FC, and a battery as inputs controlled a DC motor. The combination of renewable energy sources made the system operate with high reliability and without any pollution. A decentralized control method was proposed, which is a well-known multivariable control technique. This control system did not need a decoupling network. Furthermore, there was no need for feedback from all state variables, which reduced the number of sensors. This reduction in the number of sensors led to a simple implementation and an inexpensive controller. A high number of sensors in converters utilizing the voltage boosting technique is crucial because the number of elements is increased. The use of the pole placement control technique, which imposes many sensors, is not logical. In contrast, due to the small number of sensors, the decentralized control technique can be helpful for such converters, which has been discussed in detail in this paper.

Data Availability

Data openly available in a public repository that issues datasets with DOIs.

Conflicts of Interest

The authors declare that they have no conflicts of interest.

References

[1] F. Nejabatkhah, S. Danyali, S. H. Hosseini, M. Sabahi, and S. M. Niapour, "Modeling and control of a new three-input DC–DC boost converter for hybrid PV/FC/battery power system," *IEEE Transactions on Power Electronics*, vol. 27, no. 5, pp. 2309–2324, 2012.

[2] Z. Qian, O. Abdel-Rahman, and I. Batarseh, "An integrated four-port DC/DC converter for renewable energy applications," *IEEE Transactions on Power Electronics*, vol. 25, no. 7, pp. 1877–1887, 2010.

[3] S. Danyali, S. H. Hosseini, and G. B. Gharehpetian, "New extendable single-stage multi-input DC–DC/AC boost converter," *IEEE Transactions on Power Electronics*, vol. 29, no. 2, pp. 775–788, 2014.

[4] N. Zhang, D. Sutanto, and K. M. Muttaqi, "A buck-boost converter based multi-input DC-DC/AC converter," in *Proceedings of the IEEE International Conference on Power System Technology (POWERCON)*, IEEE, Wollongong, NSW, Australia, September 2016.

[5] F. Kardan, R. Alizadeh, and M. R. Banaei, "A new three input DC/DC converter for hybrid PV/FC/battery applications," *IEEE Journal of Emerging and Selected Topics in Power Electronics*, vol. 5, no. 4, pp. 1771–1778, 2017.

[6] J. Hui, A. Bakhshai, and P. K. Jain, "A hybrid wind-solar energy system: a new rectifier stage topology," in *Proceedings of the Twenty-Fifth Annual IEEE Applied Power Electronics Conference and Exposition (APEC)*, IEEE, Palm Springs, CA, USA, February 2010.

[7] A. Khaligh, J. Cao, and Y.-J. Lee, "A multiple-input DC–DC converter topology," *IEEE Transactions on Power Electronics*, vol. 24, no. 3, pp. 862–868, 2009.

[8] S. Hosseini, F. Nejabatkhah, and S. Danyali, "Grid connected Hybrid PV/FC/Battery power system based on cascade H-bridge multilevel inverter," *in Proceedings of the IEEE EPEC, Canada*, pp. 1036–1041, 2011.

[9] S. H. Hosseini, S. Danyali, F. Nejabatkhah, and S. A. M. Niapoor, "Multi-input DC boost converter for grid connected hybrid PV/FC/battery power system," in *Proceedings of the IEEE Electrical Power and Energy Conference*, IEEE, Halifax, NS, Canada, August 2010.

[10] H.-L. Do, "A zero-voltage-switching DC– DC converter with high voltage gain," *IEEE Transactions on Power Electronics*, vol. 26, no. 5, pp. 1578–1586, 2011.

[11] H. Krishnaswami and N. Mohan, "Three-port series-resonant DC–DC converter to interface renewable energy sources with bidirectional load and energy storage ports," *IEEE Transactions on Power Electronics*, vol. 24, no. 10, pp. 2289–2297, 2009.

[12] H. Tao, A. Kotsopoulos, J. Duarte, and M. Hendrix, "Family of multiport bidirectional DC–DC converters," *IEE Proceedings—Electric Power Applications*, vol. 153, no. 3, pp. 451–458, 2006.

[13] R.-J. Wai, C.-Y. Lin, and Y.-R. Chang, "High step-up bidirectional isolated converter with two input power sources," *IEEE Transactions on Industrial Electronics*, vol. 56, no. 7, pp. 2629–2643, 2009.

[14] R. Wai, C. Lin, L. Liu, and Y. Chang, "High-efficiency single-stage bidirectional converter with multi-input power sources," *IET Electric Power Applications*, vol. 1, no. 5, pp. 763–777, 2007.

[15] A. Khaki-Sedigh and B. Moaveni, *Control configuration selection for multivariable plants*, Springer, Berlin, Germany, 2009.

[16] A. Alizadeh Asl and R. Alizadeh Asl, "Modeling and control of a hybrid DC/DC/AC converter to transfer power under different power management strategies," *International*

Journal of Power Electronics and Drive Systems, vol. 12, no. 3, p. 1620, 2021.

[17] A. A. Asl, R. A. Asl, N. V. Kurdkandi, and S. H. Hosseini, "Modelling and controlling a new PV/FC/battery DC–DC converter suitable for DC motor," *Journal of Engineering*, vol. 2022, no. 6, 582 pages, Article ID 12138, 2022.

[18] P. Mohseni, S. Hossein Hosseini, M. Maalandish, and M. Sabahi, "Ultra-high step-up two-input DC–DC converter with lower switching losses," *IET Power Electronics*, vol. 12, no. 9, pp. 2201–2213, 2019.

[19] P. Mohseni, S. H. Hosseini, M. Sabahi, and M. Maalandish, "A multi-input-single-output high step-up DC-DC converter with low-voltage stress across semiconductors," *International Transactions on Electrical Energy Systems*, vol. 29, no. 12, Article ID e12123, 2019.

[20] P. Mohseni, S. H. Hosseini, M. Sabahi, T. Jalilzadeh, and M. Maalandish, "A new high step-up multi-input multi-output DC–DC converter," *IEEE Transactions on Industrial Electronics*, vol. 66, no. 7, pp. 5197–5208, 2019.

[21] R. R. Ahrabi, H. Ardi, M. Elmi, and A. Ajami, "A novel step-up multiinput DC–DC converter for hybrid electric vehicles application," *IEEE Transactions on Power Electronics*, vol. 32, no. 5, pp. 3549–3561, 2017.

[22] F. Akar, Y. Tavlasoglu, E. Ugur, B. Vural, and I. Aksoy, "A bidirectional nonisolated multi-input DC–DC converter for hybrid energy storage systems in electric vehicles," *IEEE Transactions on Vehicular Technology*, vol. 65, no. 10, pp. 7944–7955, 2016.

[23] M. R. Banaei, H. Ardi, R. Alizadeh, and A. Farakhor, "Non-isolated multi-input–single-output DC/DC converter for photovoltaic power generation systems," *IET Power Electronics*, vol. 7, no. 11, pp. 2806–2816, 2014.

[24] V. Marzang, S. H. Hosseini, N. Rostami, P. Alavi, P. Mohseni, and S. M. Hashemzadeh, "A high step-up nonisolated DC–DC converter with flexible voltage gain," *IEEE Transactions on Power Electronics*, vol. 35, no. 10, pp. 10489–10500, 2020.

[25] S. Mohammadi, M. Dezhbord, M. Babalou, and S. H. Hosseini, "A new non-isolated multi-input DC-DC converter with high voltage gain and low average of normalized peak inverse voltage," in *Proceedings of the 10th International Power Electronics, Drive Systems and Technologies Conference (PEDSTC)*, IEEE, Shiraz, Iran, February 2019.